Structural and Multidisciplinary Optimization (2026) 69:119
https://doi.org/10.1007/s00158-026-04312-y

RESEARCH PAPER

Length scale control for level set-based topology optimization through spread skeletons

N. Hermann[1] · **L. Noël**[1]

Received: 5 December 2025 / Revised: 4 March 2026 / Accepted: 10 March 2026

Abstract

This paper presents an efficient and easy-to-implement method for imposing feature size in level set-based topology optimization. A minimum length scale is enforced via a penalty based on a spread skeleton that captures the location of the skeleton and the required distance to it. The skeleton is constructed using first-order gradient information by solving a heat conduction problem and smoothing the resulting gradient with a PDE-based filter. Unlike other approaches, the method does not require to carry out integration over the skeleton, construct additional integration domains, or build an accurate distance from the skeleton. The work focuses on the generation of spread skeletons and the influence of the formulated penalty on optimization results. The design geometry is represented by a level set function, and structural responses are predicted using the extended finite element method. Optimization problems are solved using gradient-based algorithms, and the sensitivity analysis is performed with the adjoint approach. The ability of the proposed method to accurately control length scale is demonstrated with compliance minimization problems under a volume constraint. Similarly to other feature size control schemes, the developed geometric penalty tends to inhibit topological changes, especially in two dimensions, and results in a high dependence on the initial layout. An activation strategy that successively recruits regions of the design domain based on the spread skeleton value is used to avoid early convergence to suboptimal solutions. Numerical examples demonstrate the potential of the proposed framework to generate designs exhibiting both enhanced performance and a minimum length scale.

Keywords Level set · Immersed boundary method · Topology optimization · Length scale · Skeleton

1 Introduction

Since early work by Bendsøe and Kikuchi (1988), topology optimization (TO) has been used as a systematic tool for the generation of high-performance designs satisfying a broad range of requirements, see Sigmund and Maute (2013) and Deaton and Grandhi (2014). Despite its adoption within industry, resulting designs are often regarded as conceptual and require postprocessing to ensure their manufacturability. However, altering optimized designs might significantly affect their performance. Therefore, considerable efforts have been focused on including manufacturing constraints early on during the optimization process, see Lazarov et al. (2016); Vatanabe et al. (2016), and Liu and Ma (2016).

Among other fabrication aspects, feature size control quickly became a topic of interest in TO and is still being investigated to date. Reasons behind this continuous research are manifold. Imposing geometric restrictions allows matching manufacturing constraints, such as, e.g., the size of a print nozzle or a cutting tool, and has a direct impact on the design geometry in terms of complexity and level of redundancy (Sigmund 2009; Guest 2009a). Furthermore, enforcing a minimum length scale is highly desirable from a numerical perspective as it allows for an appropriate choice of the discretization and guarantees that physics responses on the finest parts of the design are resolved accurately.

The development of feature size control in TO was initially driven by the need to address checkerboard and mesh dependency issues in density-based approaches and can be traced back to the introduction of filtering techniques by Sigmund (1997); Bourdin (2001), and Bruns and Tortorelli (2001). The basic idea is to apply blurring techniques, derived from image

Responsible Editor: Gregoire Allaire.

✉ N. Hermann
n.hermann@tudelft.nl

[1] Department of Precision and Microsystems Engineering, Delft University of Technology, Mekelweg 2, Delft 2628, CD, The Netherlands

Published online: 27 April 2026

processing, to introduce a length scale below which design variations are discouraged. As filtering does not guarantee a minimum length scale, different restrictions were introduced, for example, to control the gradient (Petersson and Sigmund 1998) or the monotonicity (Poulsen 2003) of the density field. To tackle the introduction of intermediate densities after filtering, Guest et al. (2004) proposed to project the density field to obtain black and white designs with minimum length scale. The projection, based on the Heaviside step function, defines an element as solid when the average density in its neighborhood is larger than a minimum value, thus satisfying length scale in the solid.

Filtering and projection approaches gained in popularity and multiple projection techniques were introduced to achieve, for example, a minimum length scale in the solid and in the void simultaneously (Guest 2009b), a maximum length scale in the solid (Guest 2009a), and a minimum and maximum length scale in the solid and in the void (Carstensen and Guest 2018). To address the issue of robustness against manufacturing uncertainties and artificially stiff so-called one-node connected hinges, Sigmund (2009) proposed the robust formulation. The approach relies on two projections that erode and dilate the design and use a min/max formulation to guarantee the performance of the resulting eroded, intermediate, and dilated layouts. Wang et al. (2011) modified the approach by adding a projection for the intermediate design for a more stable convergence of the optimization problem. Despite the additional cost associated with the analysis of multiple designs, the robust approach is commonly used in practice and is still being further developed. Among others, Schevenels et al. (2011) account for non-uniformity in the erosion and dilation operators, Fernández et al. (2020) add simultaneous control of the maximum in the solid and the minimum length scale in the void, and Mommeyer et al. (2024) use Taylor series approximations to speed up the required analyses.

In level set-based TO, the design geometry is defined by the iso-contours of one or multiple level set functions (LSF), see van Dijk et al. (2013), leading to a crisp description of design boundaries. Length scale control can be achieved using geometric information conveniently provided by the LSF. Chen et al. (2008) and Luo et al. (2008) control the interaction between points lying on the design boundary within a prescribed distance of each other. The penalty minimization promotes the development of strip-like features with minimum length scale. Liu et al. (2016) prescribe a minimum length scale in the void for rough-to-finish manufacturing. Rough machining is enabled by constraining peak values of the distance from the design boundary in the void, while finish machining is achieved by limiting the minimum curvature on the design boundary. In Yamada (2019b), geometric shape features, including thickness, orientation, or skeleton location, are extracted from an extended normal field to the design boundary. The latter is obtained by solving a fictitious physical problem, i.e., one steady-state diffusion equation per space dimension, over the design domain. In Yamada (2019a), a length scale constraint is formulated by integrating the thickness measure over the design area. Michailidis (2014) and Allaire et al. (2016) generate offset areas between the design boundary and a curve lying at a given distance from it. Over these areas, the signed distance to the design boundary is constrained to impose minimum and maximum length scale in the solid and minimum length scale in the void. Wang et al. (2016) control length scale by minimizing the difference between a geometric and a level set offset area, i.e., the area created between the zero iso-contour and a given distance iso-contour of the LSF. Contrary to the level set offset area, the geometric one includes overlapping regions and is evaluated based on the curvature of the design boundary. In these approaches, feature size control is enforced via constraints and penalties, which tend to inhibit topological changes and might increase the dependence on the initial layout.

With the emergence of hybrid TO approaches combining geometry representations, see Barrera et al. (2020); Wei et al. (2020), and Stankiewicz et al. (2021) among others, techniques originally developed for density-based TO can now be exploited in, for example, level set-based TO. Building directly upon filtering techniques, Barrera et al. (2022) impose length scale in level set-based TO by using a derived or an additional filtered density field. In Andreasen et al. (2020) and Aage et al. (2021), a density field is derived from the level set field and length scale is achieved following the robust design approach. In comparison with purely level set-based formulations, hybrid approaches show potential to promote topological changes.

Another popular approach to achieve length scale in TO relies on the use of skeletons. In the field of image processing, skeletons offer a simple geometric representation of arbitrary shapes and describe a set of points within an arbitrary shape that are in the closest vicinity to at least two boundary points (Siddiqi and Pizer 2008; Saha et al. 2016). In the context of feature size in TO, skeletons should ensure shape reconstructibility, that is, the capability to restore the original shape provided the skeleton and associated thickness. While not strictly necessary, additional properties are relevant when solving design problems. It is preferable to obtain a differentiable skeleton for gradient-based algorithms (Menten et al. 2023). Additionally, for a smooth convergence of the optimization problem, skeletons should be robust against small design changes and exhibit a low sensitivity to boundary fluctuations. Such a robustness can be achieved, for example, by pruning skeletons, i.e., cutting off branches that are less significant for reconstructibility (Montero and Lang 2012).

The level set method is particularly well suited to generate skeletons starting from the information provided by the LSF. In most approaches, skeletons are built using second-

order information, i.e., the Laplacian of the distance from the design boundary. In Guo et al. (2014) and later in Geiss (2018), a narrow-band skeleton is built by thresholding the Laplacian of the distance from the design boundary. Feature size is achieved by constraining the distance from the design boundary on the skeleton. The width of the obtained skeleton influences the achievable length scale, which is only exact for infinitely fine discretizations. Xia and Shi (2015) additionally prune the skeleton, built from the Laplacian of the distance from the design boundary, to eliminate less relevant branches. Length scale is then enforced by constraining the distance from the skeleton on the design boundary. To generate structures with uniform thickness without a preset target, Liu et al. (2015, 2018) penalize the distance from the design boundary when it is larger or smaller than the average thickness, evaluated using the distance from the skeleton. It should be noted that skeletons are modified along with design changes. However, this dependency is not always well defined, see Allaire et al. (2016), and is often neglected when performing sensitivity analysis. To avoid evaluating the sensitivity of the skeleton to design changes, Wang et al. (2025) propose a constraint-free formulation that enforces length scale by directly adjusting bounds on the design variables. The adjustment is based on a search strategy, in which skeleton points are identified by discontinuities in the gradient of the distance from the design boundary.

Skeleton-based formulations have also been proposed for density approaches and mainly focus on the identification of areas where the density distribution is penalized or constrained. Zhang et al. (2014) enforce minimum and maximum length scale by constraining the density to be one within a minimum distance from the skeleton or zero at distance larger than a set threshold away from the skeleton. The skeleton is generated by successive pixel deletion and its sensitivity to design changes is neglected. In Zhou et al. (2015), two skeleton-like identifier fields are derived directly from the density distribution and its gradient. To achieve minimum length scale, the density is constrained, following the robust formulation, on areas flagged by the identifier fields. Their derivatives with respect to the density are included in the sensitivity analysis. This approach was subsequently adapted to level set-based TO in Dunning (2018) and Jansen (2019). Zobaer and Sutradhar (2023) construct the skeleton by thresholding the Laplacian of the density field and reconnecting separated parts through line extrapolation and intersection. Length scale is imposed by constraining the density field similarly to Zhang et al. (2014). Huang and Liu (2024) generate uniform thickness designs by including skeleton information in the material interpolation scheme, similar to the coating approach in Clausen et al. (2015). The skeleton is obtained by thresholding the Laplacian of the distance from the design boundary followed by a filtering and a projection operation.

This paper proposes a framework to impose minimum length scale in level set-based TO using spread skeletons. The design geometry is described with a LSF. The structural analysis is based on an immersed boundary technique, here the extended finite element method (XFEM), with a generalized Heaviside enrichment strategy. Minimum feature size is enforced using a spread skeleton that embeds its location and thickness information. The latter is constructed from first-order gradient information by solving a transient heat conduction problem, followed by a smoothing to a predefined thickness matching the required length scale. For computational efficiency, a single time step is used for the transient problem. A penalty function is formulated from the spread skeleton measure and evaluated at the design boundary. To promote topological changes in the early design stage, an activation strategy is proposed for the penalty. Optimization problems are solved with gradient-based algorithms and the required derivatives of the objective and constraint functions are evaluated by the adjoint method using a semi-analytical approach. The capabilities of the proposed framework are demonstrated with two- and three-dimensional benchmark problems considering compliance minimization of solid/void designs under a volume constraint.

The remainder of the paper is organized as follows. Section 2 presents the level set description of the geometry, provides a concise overview of the basic concepts of the XFEM, and introduces the considered physics, here linear elasticity. In Sect. 3, the formulation of the optimization problems is discussed. The framework for imposing minimum length scale via a spread skeleton measure is explained. In Sect. 4, the length scale penalty is studied with two- and three-dimensional compliance minimization problems. The optimization problem and the proposed penalty are investigated, including variations of the targeted length scale, of the penalty activation strategy, and of the initial configuration. Finally, Sect. 5 draws conclusions about the developed approach to length scale control and looks at perspectives for future research.

2 Geometry and physics

In this section, the basics of the chosen XFEM-level set framework are recalled. First, the description of the design geometry using the level set method is addressed in Subsec. 2.1. Subsec. 2.2 focuses on the use of the XFEM to predict the design responses. Finally, the physics tackled in this paper, i.e., infinitesimal strain linear elasticity, and associated governing equations are presented in Subsec. 2.3.

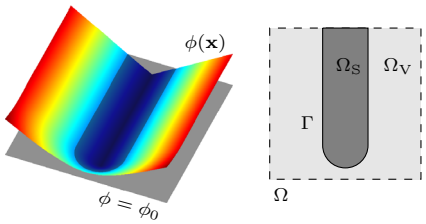

Fig. 1 Geometry description for a solid/void problem: LSF $\phi(\mathbf{x})$ and iso-level ϕ_0 (left) and resulting geometry of the design (right)

2.1 Geometry description

The level set method was introduced by Osher and Sethian (1988) as an efficient method to track propagating fronts. It was quickly adopted within the optimization community to conveniently describe the geometry of evolving designs, see van Dijk et al. (2013) for a general introduction.

A LSF $\phi(\mathbf{x})$ defines the boundary Γ of a design using an iso-level ϕ_0

$$\phi(\mathbf{x}) \begin{cases} < \phi_0, & \forall\, \mathbf{x} \in \Omega_V, \\ > \phi_0, & \forall\, \mathbf{x} \in \Omega_S, \\ = \phi_0, & \forall\, \mathbf{x} \in \Gamma, \end{cases} \tag{1}$$

where $\mathbf{x}$ are the spatial coordinates. The design boundary Γ separates the domain Ω into a solid region Ω_S and a void region Ω_V, such that $\Omega = \Omega_S \cup \Omega_V$ and $\Omega_S \cap \Omega_V = \emptyset$. This is illustrated in Fig. 1 for a solid/void problem.

The LSF is discretized to perform numerical analyses and approximated using

$$\phi(\mathbf{x}) \approx \phi^h(\mathbf{x}) = \sum_{i=1}^{I} B_i(\mathbf{x})\, \phi_i, \tag{2}$$

where I is the number of basis functions $B_i(\mathbf{x})$ and ϕ_i is the associated coefficient.

Contrary to the traditional approach, see Sethian and Wiegmann (2000); Wang et al. (2003), and Allaire et al. (2004), where the LSF is updated though solving Hamilton–Jacobi-type equations, the LSF is defined, in this work, as an explicit function of the design variables, i.e., the basis coefficients ϕ_i defined in Eq. (2), and is updated using mathematical programming methods relying on shape sensitivity information.

2.2 XFEM analysis

Immersed boundary methods allow for a crisp description of the design boundary and for an accurate resolution of the physics around it. In particular, the XFEM was introduced by Mommeyer et al. (2024) and Belytschko and Black (1999) to model crack propagation and to support the representation of strong and weak discontinuities by enriching traditional finite element approximations.

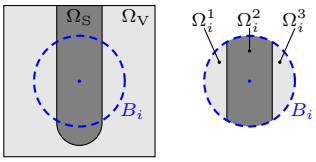

Fig. 2 Enrichment strategy for a solid/void problem: Basis function support (left) and identification of connected subregions Ω_i^j with $j = 1, 2, 3$ within the basis function support (right)

In this paper, the enrichment strategy proposed in Makhija and Maute (2014) and further extended in Noël et al. (2022) is adopted to avoid spurious coupling between disconnected subregions filled with the same material. A generalized Heaviside enrichment strategy is used and a state variable field $\mathbf{u}(\mathbf{x})$ is discretized and approximated as

$$\mathbf{u}(\mathbf{x}) \approx \mathbf{u}^h(\mathbf{x}) = \sum_{i=1}^{I} \sum_{j=1}^{J_i} B_i(\mathbf{x})\, \varphi_i^j(\mathbf{x})\, u_i^j, \tag{3}$$

where I is the number of basis functions $B_i(\mathbf{x})$ and J_i is the number of enrichment levels associated with subregions Ω_i^j in the support of a basis function $B_i(\mathbf{x})$. The coefficient u_i^j is associated with a basis function $B_i(\mathbf{x})$ and a subregion Ω_i^j within its support. The indicator function $\varphi_i^j(\mathbf{x})$ defines whether a point within the support of a basis $B_i(\mathbf{x})$ belongs to a specific connected subregions Ω_i^j such that

$$\varphi_i^j(\mathbf{x}) = \begin{cases} 1, & \text{if } \mathbf{x} \in \Omega_i^j, \\ 0, & \text{otherwise.} \end{cases} \tag{4}$$

The enrichment strategy is illustrated in Fig. 2 for a solid/void problem. Three connected subregions Ω_i^1, Ω_i^2, and Ω_i^3 are identified within the support of the basis function B_i and three enrichment levels, $J_i = 3$, are necessary.

2.3 Governing equations

The ability to enforce specific length scale is demonstrated on design problems restricted to infinitesimal strain linear elasticity. The governing equations are solved for static equilibrium and are presented in the weak form in this subsection.

Using the XFEM, the weak form of the governing equations, i.e., the total residual $R^{\mathbf{u}}$, consists of four terms

$$R^{\mathbf{u}} = R^{\mathbf{u}}_{\mathrm{E}} + R^{\mathbf{u}}_{\mathrm{D}} + R^{\mathbf{u}}_{\mathrm{G}} + R^{\mathbf{u}}_{\mathrm{K}} = 0. \tag{5}$$

The first term $R_{\mathrm{E}}^{\mathbf{u}}$ describes the balance of momentum for a linear elastic solid undergoing infinitesimal strain

$$R_{\mathrm{E}}^{\mathbf{u}} = \int_{\Omega_{\mathrm{S}}} \left(\boldsymbol{\epsilon}(\mathbf{v}) : \boldsymbol{\sigma}(\mathbf{u}) + \mathbf{v} \cdot \bar{\mathbf{b}} \right) d\Omega + \int_{\Gamma_{\mathrm{N}}} \mathbf{v} \cdot \bar{\mathbf{t}} \, d\Gamma, \tag{6}$$

where $\mathbf{u}$ and $\mathbf{v}$ are the displacement field and the associated trial field. The strain tensor, under the assumption of infinitesimal strain, is computed as $\boldsymbol{\epsilon} = \frac{1}{2}(\nabla \mathbf{u} + \nabla \mathbf{u}^{\top})$. The Cauchy stress tensor $\boldsymbol{\sigma}$ is given as $\boldsymbol{\sigma} = \mathbf{C} : \boldsymbol{\epsilon}$, with the Hooke's tensor $\mathbf{C}$. Imposed body loads are denoted $\bar{\mathbf{b}}$ and surface tractions $\bar{\mathbf{t}}$ are imposed on the Neumann boundary Γ_{N}.

The second term $R_{\mathrm{D}}^{\mathbf{u}}$ of the total residual allows for the weak enforcement of Dirichlet boundary conditions via the unsymmetric version of Nitsche's method, see Nitsche (1971).

$$\begin{aligned} R_{\mathrm{D}}^{\mathbf{u}} = &- \int_{\Gamma_{\mathrm{D}}} \mathbf{v} \cdot \left(\boldsymbol{\sigma}(\mathbf{u}) \cdot \mathbf{n} \right) d\Gamma \\ &+ \int_{\Gamma_{\mathrm{D}}} \left(\boldsymbol{\sigma}(\mathbf{v}) \cdot \mathbf{n} \right) \cdot \left(\mathbf{u} - \bar{\mathbf{u}} \right) d\Gamma \\ &+ \int_{\Gamma_{\mathrm{D}}} \gamma_{\mathrm{D}} \frac{E}{h_{\mathrm{P}}} \mathbf{v} \cdot \left(\mathbf{u} - \bar{\mathbf{u}} \right) d\Gamma, \end{aligned} \tag{7}$$

where Γ_{D} is the Dirichlet boundary with outward unit normal $\mathbf{n}$. The imposed displacements are denoted $\bar{\mathbf{u}}$. The penalty parameter γ_{D} is chosen to achieve a certain accuracy on the imposition of the boundary condition and is multiplied by the ratio of the Young's modulus E of the solid and the element edge length h_{P}.

Immersed boundary methods, such as the XFEM, are known to suffer from poor conditioning of the system of equations, especially when boundaries generate small solid subregions within a basis function support. To alleviate this issue, the face-oriented ghost penalty proposed in Burman (2010) and extended in Noël et al. (2022) is adopted in this work. The third term $R_{\mathrm{G}}^{\mathbf{u}}$ of the total residual is the ghost penalty contribution and is defined as

$$R_{\mathrm{G}}^{\mathbf{u}} = \sum_{F} \int_{F} \gamma_{\mathrm{G}} \, E h_{\mathrm{P}} \, [\![\nabla \mathbf{v} \cdot \mathbf{n}]\!] \cdot [\![\nabla \mathbf{u} \cdot \mathbf{n}]\!] \, d\Gamma, \tag{8}$$

where F is a ghost facet, i.e., an element face cut by the boundary. The jump operator $[\![\bullet]\!]$ evaluates the jump of a quantity between two elements $+$ and $-$ adjacent to the facet, such that $[\![\bullet]\!] = \bullet_{+} - \bullet_{-}$. The ghost penalty parameter is denoted γ_{G}.

As the design boundaries evolve through the optimization process, solid subregions can disconnect from the Dirichlet boundary Γ_{D}. Such free-floating subregions lead to a singular system of equations, as their rigid body modes are not constrained. The selective spring strategy proposed in Villanueva and Maute (2014) and Geiss and Maute (2018) is used in this work. The fourth term $R_{\mathrm{K}}^{\mathbf{u}}$ of the total residual is an additional stiffness applied only to free-floating solid subregions.

$$R_{\mathrm{K}}^{\mathbf{u}} = \int_{\Omega_{\mathrm{S}}} \gamma_{\mathrm{K}} \frac{E}{h_{\mathrm{P}}^2} \mathbf{v} \cdot \mathbf{u} \, d\Omega. \tag{9}$$

Solid subregions disconnected from the Dirichlet boundary are detected using an auxiliary heat conduction problem. The activation function γ_{K} takes the value one for free-floating solid subregions and zero, otherwise, following

$$\gamma_{\mathrm{K}} = \frac{1}{2}\left(1 + \tanh\left(\beta_{\mathrm{K}}(T - T_{\mathrm{th}})\right)\right), \tag{10}$$

where T is the temperature for the auxiliary heat conduction problem; T_{th} and β_{K} are the projection threshold and sharpness and are set to 0.99 and 1000, respectively.

The numerical integration of the governing equations on elements cut by the design boundary requires a specific treatment. A conforming integration mesh is generated to perform the integration accurately. Quadrangles and hexahedra are subdivided into conforming triangles and tetrahedra in two and three dimensions, respectively. For further details on the XFEM implementation, the reader is referred to Villanueva and Maute (2014); Noël et al. (2022), and Wunsch et al. (2025).

3 Optimization problem

In this paper, the approach proposed to generate designs with a minimum length scale is studied on compliance minimization problems with a volume constraint. The generic form of such optimization problems is given as

$$\begin{aligned} &\min_{\mathbf{s}} \; z(\mathbf{s}, \mathbf{u}(\mathbf{s})) \\ &\text{s.t.} \;\; g_j(\mathbf{s}, \mathbf{u}(\mathbf{s})) \leq 0, \;\; j = 1, \ldots, N_{\mathrm{g}}, \\ &\qquad \underline{s} \leq s_i \leq \bar{s}, \qquad i = 1, \ldots, N_{\mathrm{s}}, \end{aligned} \tag{11}$$

where $z(\mathbf{s}, \mathbf{u}(\mathbf{s}))$ is one of the objective function, $g_j(\mathbf{s}, \mathbf{u}(\mathbf{s}))$ is one of the N_{g} constraints, and s_i is one of the N_{s} optimization variables with its lower $\underline{s}$ and upper $\bar{s}$ bounds.

In this work, the objective function $z(\mathbf{s}, \mathbf{u}(\mathbf{s}))$ consists of four contributions

$$\begin{aligned} z(\mathbf{s}, \mathbf{u}(\mathbf{s})) = &\, w_f \frac{\mathcal{F}(\mathbf{s}, \mathbf{u}(\mathbf{s}))}{\mathcal{F}^0} \\ &+ w_r \frac{\mathcal{P}_r(\mathbf{s})}{\mathcal{P}_r^0} + w_p \frac{\mathcal{P}_p(\mathbf{s})}{\mathcal{P}_p^0} \\ &+ w_l \frac{\mathcal{P}_l(\mathbf{s}, \mathbf{u}(\mathbf{s}))}{\mu_l \mathcal{P}_p^0}, \end{aligned} \tag{12}$$

where $\mathcal{F}$ is the compliance. The LSF is controlled via a perimeter penalty $\mathcal{P}_p$ and a regularization penalty $\mathcal{P}_r$. Length scale control is enforced through a penalty $\mathcal{P}_l$, where μ_l is a fraction of the perimeter $\mathcal{P}_p^0$, used to control the strength of the enforcement of the requirement. Terms with superscript zero are the initial values of the corresponding terms. Weights w_f, w_r, w_p, and w_l are associated with the different contributions to the objective. Each of which is further detailed in the following subsections.

A volume constraint is enforced on the solid domain and is formulated as

$$g_1(\mathbf{s}, \mathbf{u}(\mathbf{s})) = \frac{\mathcal{V}_\mathrm{S}}{\mu_\mathrm{V}\mathcal{V}_\mathrm{T}} - 1 \leq 0, \tag{13}$$

where $\mathcal{V}_\mathrm{T}$ is the volume of the design domain, μ_V is the allowed solid volume fraction, and $\mathcal{V}_\mathrm{S}$ is the volume of the solid domain, evaluated as

$$\mathcal{V}_\mathrm{S} = \int_{\Omega_\mathrm{S}} d\Omega. \tag{14}$$

3.1 Minimum length scale

Developed within the field of image processing, skeletons offer simple representations of arbitrary shapes. They can be used along with distance measures to reconstruct the original shapes, see Siddiqi and Pizer (2008). This concept was first exploited by Guo et al. (2014) to efficiently control feature size in level set-based TO. In this paper, minimum length scale is enforced via skeleton information. A so-called spread skeleton that embeds both its location and the required distance to it is constructed and used to formulate a minimum length scale penalty. It is worth mentioning that the proposed penalty is independent of the approach chosen to build the spread skeleton. The procedure followed, in this work, for generating the spread skeleton is explained in details below. Alternative approaches based on different physics could be used to create measures similar to the spread skeleton, see, for example, Yamada (2019b).

While different approaches are available, the skeleton can be identified by the ridge of the shape, i.e., the location where the gradient of the distance from the shape boundary changes signs (Blum 1967). To locate the skeleton, an approximation of the gradient of the distance from the design boundary is obtained by solving a transient heat conduction problem assuming that the direction of heat flow aligns with the growth direction of the distance, see Belyaev and Fayolle (2015) and Crane et al. (2017). The residual of the weak form for a transient heat conduction problem is given as

$$R^\theta = \int_{\Omega_\mathrm{S}} \left(\lambda \rho^\theta c_p^\theta \frac{\partial \theta}{\partial t} + \nabla\lambda \cdot \left(\kappa^\theta \nabla\theta\right)\right) d\Omega, \tag{15}$$

where θ and λ are the temperature and the associated trial field. Properties ρ^θ, c_p^θ, and κ^θ are the density, the specific heat capacity, and the conduction selected for this problem. Zero conditions are applied at the initial time, $\theta_0 = 0.0$ on Ω_S, and a unit temperature is prescribed at the design boundary, $\overline{\theta} = 1.0$ on Γ. Equation (15) is solved only on the solid domain, where the information is needed. To increase the computational efficiency, a single time step is used, as proposed in Crane et al. (2017) and Geiss et al. (2019), leading to a cost comparable to solving a steady-state problem. The time step should be selected large enough to yield non-zero gradient over the considered domain.

Once its location is identified, the skeleton is spread to a chosen thickness r_S, equal to half the required minimum length scale, by smoothing the jump in the normalized gradient of the temperature field using a PDE-based filter. The weak form of the residual for the smoothing takes the form

$$R^\eta = \int_{\Omega_\mathrm{S}} \left(\nabla\boldsymbol{\zeta} \cdot \left(r^2 \nabla\boldsymbol{\eta}\right) + \boldsymbol{\zeta} \cdot \left(\boldsymbol{\eta} - \frac{\nabla\theta}{\|\nabla\theta\|}\right)\right) d\Omega, \tag{16}$$

where $\boldsymbol{\eta}$ and $\boldsymbol{\zeta}$ are the smoothed gradient and the associated trial field. The spreading radius is chosen as $r = r_\mathrm{S}/2\sqrt{3}$ following Lazarov and Sigmund (2011). Homogeneous Neumann boundary conditions, $\nabla\boldsymbol{\eta} \cdot \mathbf{n} = 0$, are applied on the design boundary Γ. Equation (16) is solved only on the solid domain to avoid interaction between disconnected members through the void domain.

The obtained smoothed gradient field is used to build a so-called spread skeleton $\mathcal{S}$

$$\mathcal{S} = 1 - \|\boldsymbol{\eta}\|^p, \tag{17}$$

which takes non-zero values when the minimum length scale is not satisfied and drops to zero as the thickness of a member approaches $2r_\mathrm{S}$. The operator $\|\bullet\|$ is the Euclidean norm and p is an exponent chosen as $p = 2$ to obtain a smooth measure.

The procedure to build the spread skeleton for a 1D problem is illustrated in Fig. 3. Solving Eq. (15), the temperature θ is set to one at the boundary, denoted x_Γ, and presents a minimum over the skeleton location, denoted x_Σ. The normed gradient of the temperature $\nabla\theta/\|\nabla\theta\|$ switches sign over the skeleton and serves as an identifier for its location. The jump in the normed gradient is filtered with a radius r_S leading to the smoothed gradient η used to build the spread skeleton $\mathcal{S}$.

If the spread skeleton measure $\mathcal{S}$ is zero at the design boundary, then the minimum length scale is satisfied. If not, the member is too thin and needs to be removed or thickened. To promote this behavior, a penalty $\mathcal{P}_l$ is introduced in the objective and is evaluated at the design boundary as

$$\mathcal{P}_l = \int_\Gamma \gamma_\mathrm{K}\, \mathcal{S}\, d\Gamma, \tag{18}$$

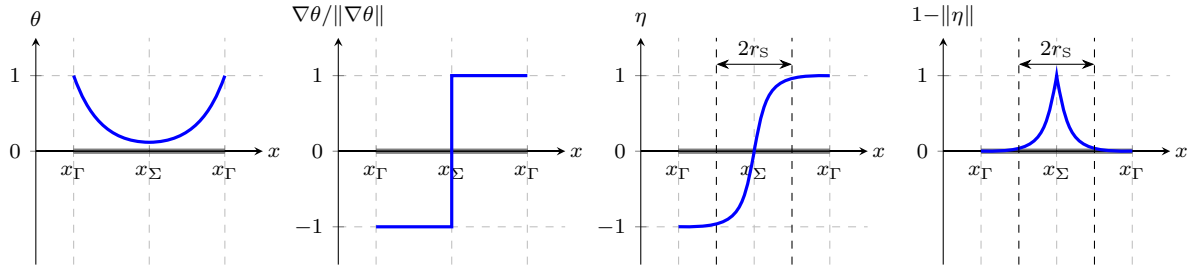

Fig. 3 Generation of a length scale control measure based on spread skeleton. From left to right, the temperature θ, the normed gradient of the temperature $\nabla\theta/\|\nabla\theta\|$, the smoothed gradient η, and the spread skeleton measure $1-\|\eta\|$

where γ_K, defined in Eq. (10), deactivates the penalty on free-floating solid islands. Contrary to other approaches available in the literature, the proposed method does not require to perform integration on the skeleton itself, to construct additional integration domains, or to build an accurate distance from the skeleton. While the feature size can be effectively and accurately controlled using the proposed spread skeleton measure through a penalty or a constraint formulation, numerical experiments showed that penalization generally leads to better performing designs, as it remains active throughout the optimization process. This approach is therefore adopted in this work.

In practice, the spread skeleton measure $\mathcal{S}$ is only approximately dropping to zero at length scale, as the domain over which the gradient is smoothed is finite, see Lazarov and Sigmund (2011). On an infinite one-dimensional domain, the smoothed gradient solution is obtained by convolution of the input gradient and the Green's function and leads to a spread skeleton

$$\mathcal{S}_a = 1 - |\eta| = \exp(-|x|/r), \tag{19}$$

where $|\bullet|$ is the absolute value operator. On finite domains, the obtained smoothed gradient deviates from Eq. (19) and becomes dependent on the actual size of the domain, see Fig. 4. To allow for an accurate feature size control, it is necessary that the spread skeleton measure approaches zero as the domain thickness approaches the required length scale. Therefore, the following correction is applied

$$\mathcal{S}_c = \frac{\sqrt{\max\left(1-\left(\frac{\|\eta\|}{\eta_c}\right)^p, 0\right)^2 + \xi^2} - \xi}{\sqrt{1+\xi^2} - \xi}, \tag{20}$$

where η_c is a correction term, chosen as $\eta_c = 0.937$, based on numerical studies of one-dimensional problems. The parameter ξ controls the transition of the penalty and is set to $\xi = 0.001$. The effect of the correction is illustrated in Fig. 4 for one-dimensional domains of different thicknesses. It should be noted that the correction is only exact, i.e., drops to zero at a distance r_S from the skeleton, for members at length scale.

In order to control the length scale, it is crucial that both the transient heat conduction in Eq. (15) and the smoothing in Eq. (16) are accurately resolved on the state variable field discretization. The non-linearity of these fields and the discontinuity of the spatial gradient at the skeleton require a sufficient number of elements over the spread radius r_S. A practical lower bound of $r_S = 1.5h_P$ is adopted in this work.

To mitigate the dependence on the initial design and promote topological changes, see Allaire et al. (2016), an activation strategy is used to gradually introduce the effect of the penalty

$$\mathcal{P}_l = \int_\Gamma \gamma_K\, \gamma_L\, \mathcal{S}_c\, d\Gamma. \tag{21}$$

The activation function γ_L successively recruits thinner and thinner members allowing them to disappear in the early design and is defined as

$$\gamma_L = \frac{1}{2}\Big(1 + \tanh\Big(-\beta_L\big(\mathcal{S}_c - \mathcal{S}_{th}\big)\Big)\Big), \tag{22}$$

where the parameters S_{th} and β_L are the projection threshold and sharpness, respectively. While the sharpness is kept constant during the optimization process, here $\beta_L = 25.0$, the threshold $\mathcal{S}_{th}$ is gradually increased from an initial $\mathcal{S}_I$ to a final $\mathcal{S}_F$ value

$$\mathcal{S}_{th} = \begin{cases} \mathcal{S}_I, & \text{if } I \le I_I, \\ \mathcal{S}_I - (\mathcal{S}_I - \mathcal{S}_F)\Big(\dfrac{I - I_I}{I_F - I_I}\Big), & \text{if } I_I < I \le I_F, \\ \mathcal{S}_F, & \text{if } I > I_F, \end{cases} \tag{23}$$

where I, I_I, and I_F are the current, the initial, and the final iteration for the continuation, respectively. The threshold values are chosen as $\mathcal{S}_I = 0.0$, to start the optimization without imposing the penalty, and $\mathcal{S}_F = 1.0$, to eventually enforce length scale on all members. More complex or effective continuation schemes are not further explored in this paper.

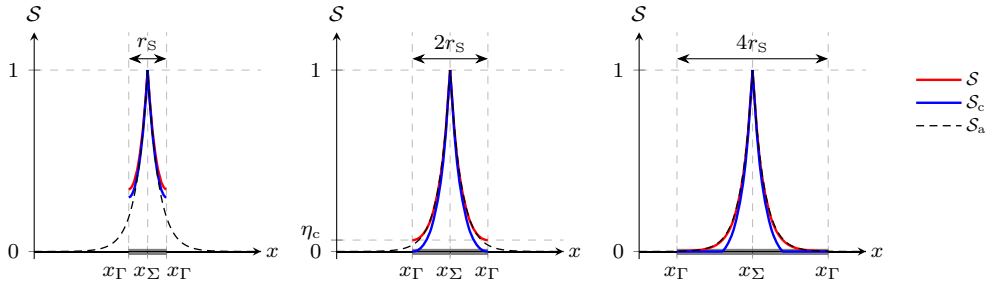

Fig. 4 Analytical $\mathcal{S}_a$ (Eq. (19)), uncorrected $\mathcal{S}$ (Eq. (17)), and corrected $\mathcal{S}_c$ (Eq. (20)) spread skeletons with $p = 1$, $\eta_c = 0.937$, and $\xi = 0.001$ for members of thickness $t = r_S,\ 2r_S,\ 4r_S$

The activation function in Eq. (22) is directly dependent on the smoothed gradient field through the corrected spread skeleton. To prevent a direct exploitation of the activation strategy to drop the length scale penalty, e.g., by generating or maintaining thin inactive structural regions within the design, the implicit dependency of the activation function on the design variables through the state variables is not included in the sensitivity analysis.

3.2 Level set regularization and perimeter penalties

In level set-based approaches, it is essential to control the level set field and its gradient to promote the generation of smooth designs and to enable a smooth convergence of the optimization process.

The second term in Eq. (12) is a level set regularization penalty, as introduced by Geiss et al. (2019). The penalty term eliminates the need for reinitialization by promoting the convergence of the level set field ϕ toward a target function $\overline{\phi}$. The target function is built from a distance field obtained through the heat method, see Crane et al. (2017), that requires solving two additional partial differential equations. The penalty is formulated as

$$\mathcal{P}_r = \frac{\int_\Omega w_\phi \left(\phi - \overline{\phi}\right)^2 d\Omega}{\int_\Omega \phi_B^2 \, d\Omega} + \frac{\int_\Omega w_{\nabla\phi} \|\nabla\phi - \nabla\overline{\phi}\|^2 d\Omega}{\int_\Omega d\Omega}, \tag{24}$$

where ϕ_B is a bound on the level set field value and where the weights w_ϕ and $w_{\nabla\phi}$ control the regularization in the vicinity and distance from the boundary, see Barrera et al. (2020).

The third term in Eq. (12) is a perimeter penalty, as proposed by Haber et al. (1996) and Makhija and Maute (2014), that mitigates the appearance of irregular geometric features and ensures a well-posed optimization problem. The perimeter is computed as

$$\mathcal{P}_p = \int_\Gamma d\Gamma. \tag{25}$$

It is recommended to allocate small weights to both penalties with respect to the main objective $\mathcal{F}$ to minimally impact the optimization problem, i.e., up to 20% for w_p (Makhija and Maute 2014) and up to 10% for w_r (Geiss et al. 2019).

4 Numerical examples

This section explores the characteristics of the proposed minimum length scale framework for level set-based TO. The assessment of the flexibility and effectiveness of the method is carried out on two- and three-dimensional compliance minimization examples under a volume constraint. Variations of the optimization problem and the length scale formulation are investigated.

In all examples, state and design variable fields are approximated with linear and quadratic B-spline functions, respectively. Coarser and higher-order discretizations are used for the design variable field, resulting in a filtering effect which promotes the generation of smoother designs and speed up the convergence of the optimization problem, see Noël et al. (2020).

In this work, physics responses consider linear elasticity, heat conduction, and filtering. Unless specified otherwise, physics parameters, introduced in Subsec. 2.3, are provided in Table 1 in self-consistent units. The forward and sensitivity analyses are implemented and carried out using the open-source C++ immersed finite element and optimization package MORIS (2025). The resulting system of discretized governing equations and adjoint sensitivity equations are solved using the Multifrontal Massively Parallel Solver (MUMPS), see Amestoy et al. (2001). The 3D problems are solved by employing a GMRES algorithm from the Trilinos software project package Belos, preconditioned by an incomplete LU factorization (ILU), see Bavier et al. (2012). A relative drop in the linear residual of 10^{-9} is required.

Optimization problems are solved with the Globally Convergent Method of Moving Asymptotes (GCMMA), see Svanberg (2002). The parameters for the initial, lower, and

Table 1 Numerical optimization examples: Physics parameters and respective Nitsche's and Ghost penalty parameter

Linear elasticity				
E	ν	$\bar{\mathbf{t}}$	$\gamma_{\mathrm{N}}^{\mathbf{u}}$	$\gamma_{\mathrm{G}}^{\mathbf{u}}$
1.0	0.3	$-1.0\mathbf{e}_{\mathrm{y}}$	10.0	0.01
Heat method				
ρ^{θ}	c_p^{θ}	κ^{θ}	$\gamma_{\mathrm{N}}^{\theta}$	$\gamma_{\mathrm{G}}^{\theta}$
1.0	0.1	10.0	10.0	0.01
Smoothed gradient				
$\gamma_{\mathrm{N}}^{\eta}$	$\gamma_{\mathrm{G}}^{\eta}$			
10.0	0.01			

Table 2 Numerical optimization examples: Optimization penalty parameters

Optimization weights			
w_f	w_p	w_r	w_l
1.0	0.1	0.05	0.05
Continuation			
I_{S}	I_{F}	I_{T}	
0	400	20	
S_{I}	S_{F}	$\mu_{\mathrm{l,I}}$	$\mu_{\mathrm{l,F}}$
0	1	1	0.025

upper asymptote adaptation are set to 0.5, 0.7, and 1.2, respectively. Optimization problems are considered converged if the objective stagnates and the constraints are satisfied. Necessary gradients of response functions are evaluated by the adjoint method, using a semi-analytical approach, following (Sharma et al. 2017). Optimization parameters, introduced in Sect 3, are given in Table 2, unless specified otherwise.

4.1 Two-dimensional beam

The design of a 2D beam with length $2L = 240$ and height $H = 40$ is investigated, see Fig. 5. The beam is supported at its bottom left corner and is subjected to a vertical traction on its top right corner. Design-independent solid blocks with side dimension $l = 1$ are introduced under the load and at the support. Exploiting symmetry, only half of the beam is considered. Symmetry boundary conditions are enforced for the structural and the smoothing problem on the symmetry axis marked in blue, $u_{\mathrm{x}} = 0$ and $\eta_{\mathrm{x}} = 0$. For the symmetry of the skeleton, Neumann boundary conditions are enforced for the heat conduction problem on the symmetry axis. The target volume fraction is set to $\mu_{\mathrm{V}} = 0.4$.

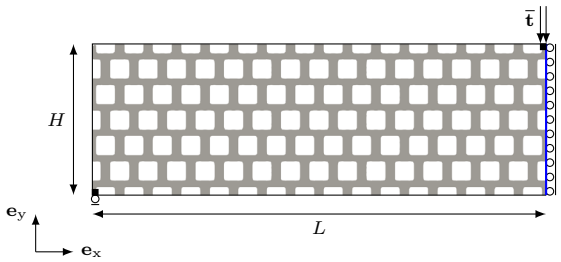

Fig. 5 2D beam design: Geometry, boundary conditions, and initial hole seeding

The state variable fields are discretized on a mesh with element size $h_{\mathrm{P}} = H/160 = 0.25$, while the design variable field is discretized with a larger element size $h_{\mathrm{D}} = H/80 = 0.5$. As design changes are driven by shape sensitivities in this work and hole nucleation is not possible, the initial design is seeded with holes. Hole seeding during the optimization could be triggered with topological derivatives or other methods, see van Dijk et al. (2013), but is not implemented here.

Throughout the optimization procedure, the relative influence of individual terms in the objective function is maintained by updating their scaling term every I_{T} iterations. To reduce the dependence on the initial configuration, the enforcement of the length scale requirement is initially relaxed and gradually tightened over the optimization process, as discussed in the following subsection.

4.1.1 Length scale activation

The introduction of length scale control penalties or constraints tends to inhibit topological changes, and there is a necessity to relax the enforcement of such requirement, especially during early optimization iterations. Various continuation approaches have been reported in the literature, both in density- and level set-based TO, see, for example, Zhou et al. (2015) and Allaire et al. (2016).

In this work, we investigate the effect of two continuation strategies: (i) a gradual strengthening of the enforcement of the length scale requirement and (ii) a progressive activation of regions of the design domain. The strengthening strategy gradually tightens the enforcement of the length scale by decreasing the perimeter fraction parameter μ_l, effectively increasing its weight within the objective, while the activation strategy successively includes regions of the design domain into the penalty based on the spread skeleton measure. Both strategies are implemented through continuations on parameters μ_l and $\mathcal{S}_{\mathrm{th}}$ that are updated every I_{T} iterations from 1 to 0.025 and from 0 to 1, respectively, following Eq. (23).

Figure 6 shows 2D beam designs with a length scale $r_{\mathrm{S}} = 0.625$, obtained without any continuation (top), with the strengthening strategy (middle), and with strengthening and

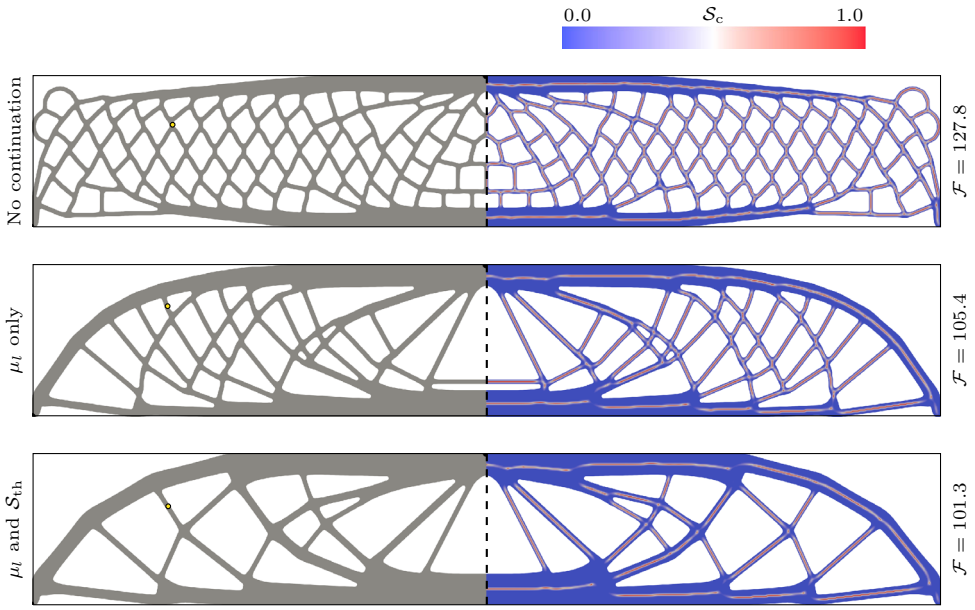

Fig. 6 2D beam design: Enforcing a length scale $r_S = 0.625$ without continuation (top), with strengthening strategy (middle) and with strengthening and activation strategies (bottom)

activation strategy (bottom). Resulting layouts are depicted on the left, while associated spread skeletons are shown on the right. A yellow mark represents the minimum length scale and performance in terms of compliance is provided for each design.

Without any relaxation of the penalty, the optimization problem results in a low-performing solution (top) with a high dependence on the initial configuration. Although the design exhibits the desired length scale, only marginal topological changes occurred. This limitation is inherent to the proposed formulation, where the length scale penalty value can only be dropped by increasing the thickness of members that fall below the imposed feature size, while breaking of members is only caused by the volume constraint. As the optimization problem is dominated by the length scale requirement, breaking of members is inhibited and structurally inferior designs are generated.

Starting the optimization with a relaxed enforcement of the length scale requirement, the optimization problem is primarily driven by the compliance, leading to more significant topological changes and an enhanced design (middle), $\mathcal{F} = 105.4$ with continuation versus 127.8 without. As the perimeter fraction parameter μ_l decreases, the emphasis in the objective shifts toward the geometric constraint, resulting in the thickening of members to the imposed length scale and ultimately in the inhibition of topological changes. It is to be noted, that in the strengthening strategy, the length scale penalty is active during the entire optimization procedure, and acts on all structural regions equally, ultimately restraining topological changes. The combined effect of the weight and perimeter fraction parameters dictates the point at which, during the optimization procedure, the length scale penalty overrules the compliance and ultimately fully inhibits topological changes.

To further promote topological changes, the continuation on the perimeter fraction parameter μ_l can be combined with an activation strategy. The penalty is initially exclusively applied to thick members, while thin ones are progressively recruited based on the spread skeleton value. As illustrated in Fig. 6, the activation strategy allows for substantial topological changes driven by the minimization of compliance. Structurally significant members increase in thickness, while less significant ones disappear. The resulting design (bottom) satisfies the length scale requirement and exhibits an increased mechanical performance, $\mathcal{F} = 101.3$ with activation versus 105.4 without.

Figure 7 shows the evolution of the design during the optimization process with snapshots at iteration $I = [100, 200, 300, 400]$. The length scale penalty is active in the blue and inactive in the orange regions of the design. Over the span of the optimization procedure, regions of the design domain are gradually recruited and thickened to the imposed length scale. The thickening of recruited areas, in combination with the volume constraint, leads to the thinning and eventually breaking of areas in which the penalty is inactive. After $I_F = 400$ iterations, the penalty is active throughout the structure and length scale is enforced everywhere. It should be noted that, once included in the penalty, members are prone to remain in the final design, as the formulation tends to inhibit topological changes. Both the activation strategy

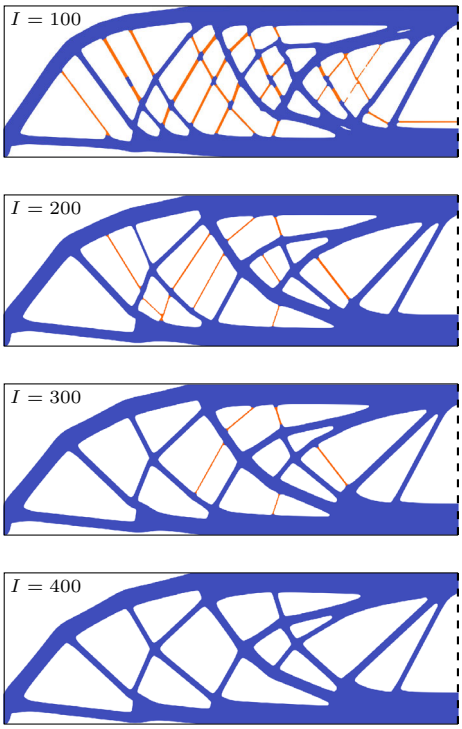

Fig. 7 2D beam design: Evolution of the design enforcing a length scale $r_S = 0.625$ with strengthening and activation strategy. Snapshots of the design are provided at iteration $I = [100, 200, 300, 400]$. Inactive regions are colored in orange, while active ones are colored in blue

and the initial configuration have a strong influence on the resulting optimized designs, see Subsec. 4.1.3 and 4.1.4 for further exploration.

4.1.2 Enforcing different length scales

In the following, the capability of the proposed formulation to accurately control the length scale is demonstrated. To this end, different minimum length scales are considered with $r_S = [0.625, 1.25, 2.5]$. Different spread radii result in different spatial gradients for the spread skeleton, i.e., larger spatial gradients for small spread radii and lower spatial gradients for large ones. To balance out this difference, the weight w_l is consistently multiplied by the ratio $r_S/0.625$.

Figure 8 shows optimized designs generated with and without length scale control. The left-hand side of the figure illustrates the design layouts, where a yellow circle indicates the imposed length scale. The right-hand side shows the associated spread skeleton. Performance in terms of compliance is provided for each design.

All three generated designs resemble the 2D beam design without geometry constraint (top), while satisfying the imposed length scale. Clear trends are observable in designs with increasing feature size. The smaller the filter radius, the larger is the non-uniformity in thickness across individual member and the closer is the resemblance to the original design. As the imposed length scale becomes larger, designs are made of fewer members with increased uniformity in thickness and, as expected, decreased performance, $\mathcal{F} = 101.3$ to 114.8 for $r_S = 0.625$ to 2.5.

Besides differences in design layouts, clear differences in the thickness and connectivity of the spread skeleton are observable. A small spread radius results in a thin and disconnected spread skeleton with large spatial gradient. While the spread skeleton is fully connected inside straight members, it is disconnected at the junctions between multiple members. This can be explained by the so-called object angle ψ, which is the angle at the skeleton point between a vector directed to the neighboring skeleton point and a vector directed to the closest boundary point, see Blum (1973) and Siddiqi and Pizer (2008). In a straight member, the approximated gradient intersects head-on at the skeleton points, that is, at an object angle of $\psi = \frac{\pi}{2}$, resulting in a clear jump in the gradient. At the junctions, the object angle is lower $\psi < \frac{\pi}{2}$, resulting in a less clear jump, and in turn, in lower spread skeleton values. This effect is amplified as the skeleton is built by means of an approximated gradient of the distance field obtained by solving Eq. (15). As reported in Crane et al. (2017), the quality of the approximated gradient depends on the selected time step, as a consequence of inherent smoothing. While full connectivity is desirable, numerical examples show that the resulting level of connectivity, even for a small spreading radius, enables the enforcement of length scale in the entire design domain.

Large spread radii result in widely diffused and connected spread skeletons with low spatial gradients. For large spread radii, it becomes visible that the proposed penalty does not only impose length scale, but also a minimum radius at junctions. For $r_S = 2.5$, the design presents curved members and rounded junctions. The spread skeleton highlights regions where the direction of the gradient of the distance to the boundary changes abruptly, which occurs not only at the skeleton points but also at junctions. As a result, sharp corners are penalized and round corners are favored. A separation in prescribing a length scale and a corner radius could be achieved by including higher-order information in the formulation, i.e., making use of the Laplacian of the distance field, which would allow distinguishing between skeleton points and junctions by means of flux direction, see Guo et al. (2014) and Geiss (2018) for representation of the Laplacian at sharp corners.

Different spread radii lead to inherently different challenges in the optimization problems. For small spread radii, a key difficulty is to promote topological changes, as the allowed maximum volume can accommodate the numerous redundant structural members present in the initial design. A slow continuation is key to initially let the structural problem control the design updates, before the penalty inhibits

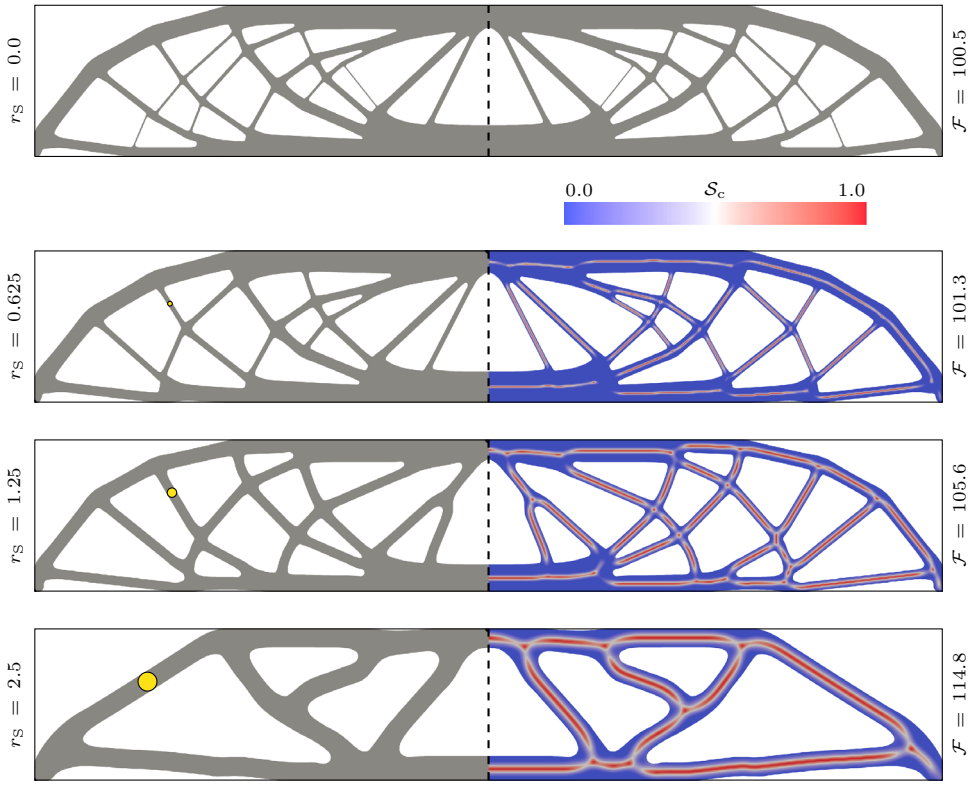

Fig. 8 2D beam design: Enforcing different length scales with spread radii $r_S = [0.0,\ 0.625,\ 1.25,\ 2.5]$ with strengthening and activation strategy

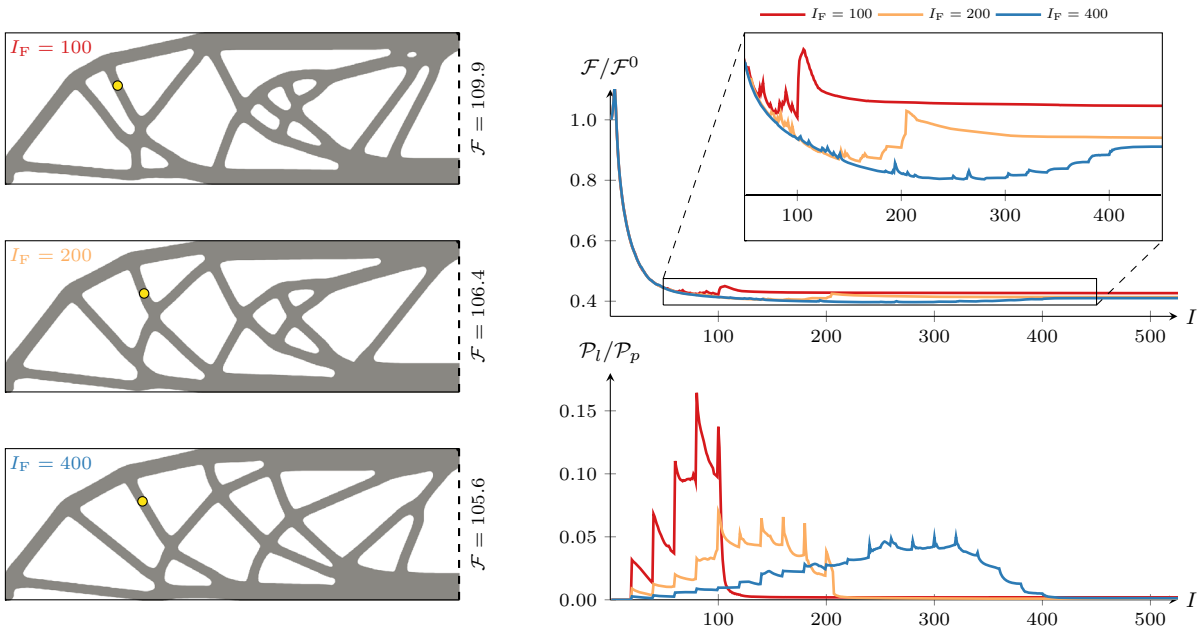

Fig. 9 2D beam design: Enforcing a length scale $r_S = 1.25$ with different final iterations $I_F = [100,\ 200,\ 400]$ for the activation strategy. Evolution of the scaled compliance $\mathcal{F}/\mathcal{F}^0$ and scaled length scale penalty $\mathcal{P}_l/\mathcal{P}_p$ throughout the optimization (right) and resulting designs (left)

topological changes. In contrast, topological changes are inevitable for large spread radii due to the limited volume. The key difficulty here is to recruit appropriate structural regions based on a topology that differs significantly from the final one. As structural regions are being recruited and thickened, inactive regions are being thinned, delaying their recruitment, and resulting in intermediate designs with wide inactive regions below length scale. As the optimization procedure progresses, the entire design is being recruited, leading to either the thickening or removal of said structural regions as a result of the limited volume. A relaxed feature size penalty, combined with a slow continuation strategy results in optimization problems, in which the thickness of numerous inactive structural regions is optimized, even though ultimately being removed, resulting in a slow convergence.

Finally, it should be noted that, despite a rather slow activation strategy with $I_\mathrm{F} = 400$, structurally suboptimal members are still present in the final designs, e.g., the split member in the center for $r_\mathrm{S} = 1.25$, or the curved member for $r_\mathrm{S} = 2.5$. This effect is further studied in the next subsection.

4.1.3 Influence of the activation strategy

As demonstrated in Subsec. 4.1.1, the use of an activation strategy is necessary for the proposed formulation to produce designs that are not fully dominated by the feature size. In this subsection, the influence of the continuation in the activation strategy on the optimization process and the resulting designs is investigated. To this end, the recruitment of design areas is carried out with three different final continuation iterations $I_\mathrm{F} = [100,\ 200,\ 400]$.

Figure 9 shows designs obtained for three different final continuation iterations on the left. A length scale of $r_\mathrm{S} = 1.25$ is enforced for all designs, as indicated by the yellow mark. Performance in terms of compliance is provided for each design. On the right-hand side, the evolution of the scaled compliance $\mathcal{F}/\mathcal{F}^0$ and scaled feature size penalty $\mathcal{P}_l/\mathcal{P}_p$ is provided. Regardless of the selected final continuation iteration, all generated designs satisfy the imposed minimum feature size. However, the choice of a final continuation iteration has clear implications on the designs and their performance.

The convergence plots show that as I_F increases, so does the total number of iterations until convergence. Although selecting a lower I_F accelerates the design process, it increases the risk of prematurely converging to suboptimal solutions. As the selection of regions subject to the length scale penalty within the design domain is accelerated, large structurally less significant regions are prone to be recruited early on and remain in the final designs. Simultaneously, the perimeter fraction parameter μ_l decreases and the incentive to thicken recruited regions is strengthened. As a result,

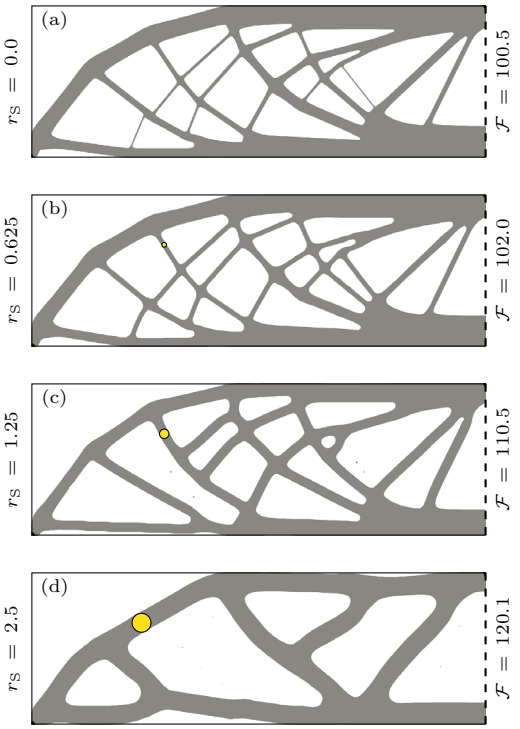

Fig. 10 2D beam design: Enforcing a length scale restarted from an unconstrained optimized layout (a), for different spread radii $r_\mathrm{S} = [0.625,\ 1.25,\ 2.5]$ (b)-(d) without strengthening and activation strategy

structurally inferior members are developed to length scale, at the cost of thinning and eventually breaking members that might be structurally more significant, but so far not recruited. This phenomenon is observable in the evolution of the compliance, as breaking a structurally relevant member leads to jumps in its value, see iterations $I = 80$ and 100 for $I_\mathrm{F} = 100$. In contrast, a slow continuation approach yields a slow, but smooth convergence of the strain energy.

The effect of a fast or slow continuation strategy emphasizes a major challenge faced by purely geometric approaches to length scale control, i.e., the limited available mechanisms to reduce the length scale penalty. Once a member is recruited, it tends to remain in the final design regardless of its contribution to the strain energy. As shown in Fig. 9, a slow activation strategy promotes topological changes by enabling the distinction between inactive regions based on their structural performance. To enforce a minimum length scale, all structural regions are recruited at the end of the optimization problem.

It should be noted that the continuation also relies on the trigger iteration I_T, as can be seen from jumps in the penalty value, as new regions of the design domain are being recruited. However, its influence on the resulting designs is less significant and is not discussed further here.

A common strategy in level set-based TO considering feature size involves (i) solving a first problem without geometric constraint and subsequently (ii) solving a second problem with geometric constraint starting from the previously optimized design, see Allaire et al. (2016) or Wang et al. (2016). The proposed activation strategy is conceptually similar to this approach. A notable distinction is that with the proposed strategy, the feature size penalty informs the entire optimization procedure, albeit significantly relaxed during early iterations. It gradually steers the optimization problem toward a solution that satisfies the length scale constraint, while considering the structural performance. In contrast, optimization problems, restarted from an unconstrained optimized layout, see Fig. 10 (a) without any continuation strategy, see Fig. 10 (b)-(d), result in designs that meet the imposed length scale, but all retain a larger number of members with reduced performance.

4.1.4 Influence of the initial configuration

In this work, design updates are driven purely by shape sensitivities, without mechanisms to nucleate new holes. To ensure adequate design freedom, the domain is seeded with multiple holes, which does not necessarily mitigate the dependence on the initial configuration. In this subsection, the effect of the length scale penalty on this dependency is investigated. Two different hole seeding patterns, with similar initial volumes, are considered, see Fig. 11 (1a) and (2a).

Figure 11 shows optimized designs without (b) and with (c)-(e) enforcing a length scale, starting from the two different initial configurations (1a) and (2a). A yellow mark denotes the imposed length scale and performance in terms of compliance is provided for each design.

Without enforcing a length scale, designs (1b) and (2b) exhibit a high degree of similarity, resulting in similar performance. However, clear differences in the local topologies are observable, indicating a convergence to different local minima. Similar observations can be made when imposing a length scale, as designs (1c), (1d), and (1e) exhibit similar topologies and performance to (2c), (2d), and (2e). However, for $r_S = 0.625$ and 1.25, the difference between results is more pronounced compared to the unconstrained designs. As observed in previous subsections, designs with a length scale show clear resemblance to the unconstrained results. Structural members below the required feature size in (c), (d), and (e) are either removed or thickened to length scale. Despite a slow continuation strategy with $I_F = 400$, structurally suboptimal members subsist in final designs, e.g., the split up members in the center of designs (1d) and (2d).

As expected, results demonstrate the inherent dependency of optimized designs on the selected initial configurations. The enforcement of a length scale seems to reinforce this dependency that is also influenced by the parameter choice for the continuation strategy.

4.2 Three-dimensional beam

In this section, the proposed length scale control approach is extended to three-dimensional space. Compared to the two-dimensional problem, the smoothing in Eq. (16) has to be solved in an extra dimension, i.e., performing a spreading of the skeleton in the $\mathbf{e}_z$-direction. In the following, the design of a 3D beam for minimal compliance under a volume constraint, equivalent to the 2D beam studied in Subsec. 4.1, is investigated.

A 3D beam with a length $2L = 240$, a height $H = 40$, and a thickness $2T = 40$ is considered, see Fig. 12. Exploiting symmetry, only a quarter of the beam is studied. The beam is supported at all corners on its bottom face and subjected to a uniformly distributed vertical traction over a rectangular area on its top face. The supports and tractions are applied over design-independent solid blocks with side dimension $l = 3$. Symmetry boundary conditions for the structural and the smoothing problem are enforced on the symmetry planes marked in blue, $u_x = u_z = 0$ and $\eta_x = \eta_z = 0$. To enforce symmetry on the skeleton, Neumann boundary conditions are imposed on the symmetry planes for the heat conduction problem. The target volume fraction is set to $\mu_V = 0.3$.

The design domain is seeded with multiple holes, see right-hand side of Fig. 12. For 3D cases, it is expected that final designs are less dependent on the initial configuration, as, contrary to 2D cases, holes can effectively be developed by varying the thickness along the third dimension. Numerical analyses are performed on meshes with an element size $h_P = T/32$ for the state variable fields and $h_D = T/16$ for the design variable field.

Contrary to the 2D case, in which the skeleton is a curve, in the 3D case, the skeleton points sit on a surface, generally referred to as a surface skeleton in the field of image processing. The spread skeleton in 3D exhibits the same information as in the 2D case, and embeds the location of the skeleton points and the required distance, allowing the reconstruction of arbitrary shapes with minimum feature size.

4.2.1 Length scale activation

For 2D problems, the activation strategy allows for the generation of designs that match the required feature size, while achieving enhanced structural performance. In this subsection, the necessity for an activation strategy is explored for 3D problems.

Optimized 3D beam designs for a length scale $r_S = 1.25$ without (left) and with (right) activation strategy with $I_F = 200$ are provided in Fig. 13. Along with the design layouts, two cuts in the $\mathbf{e}_y - \mathbf{e}_z$ plane are shown, located at a fourth and

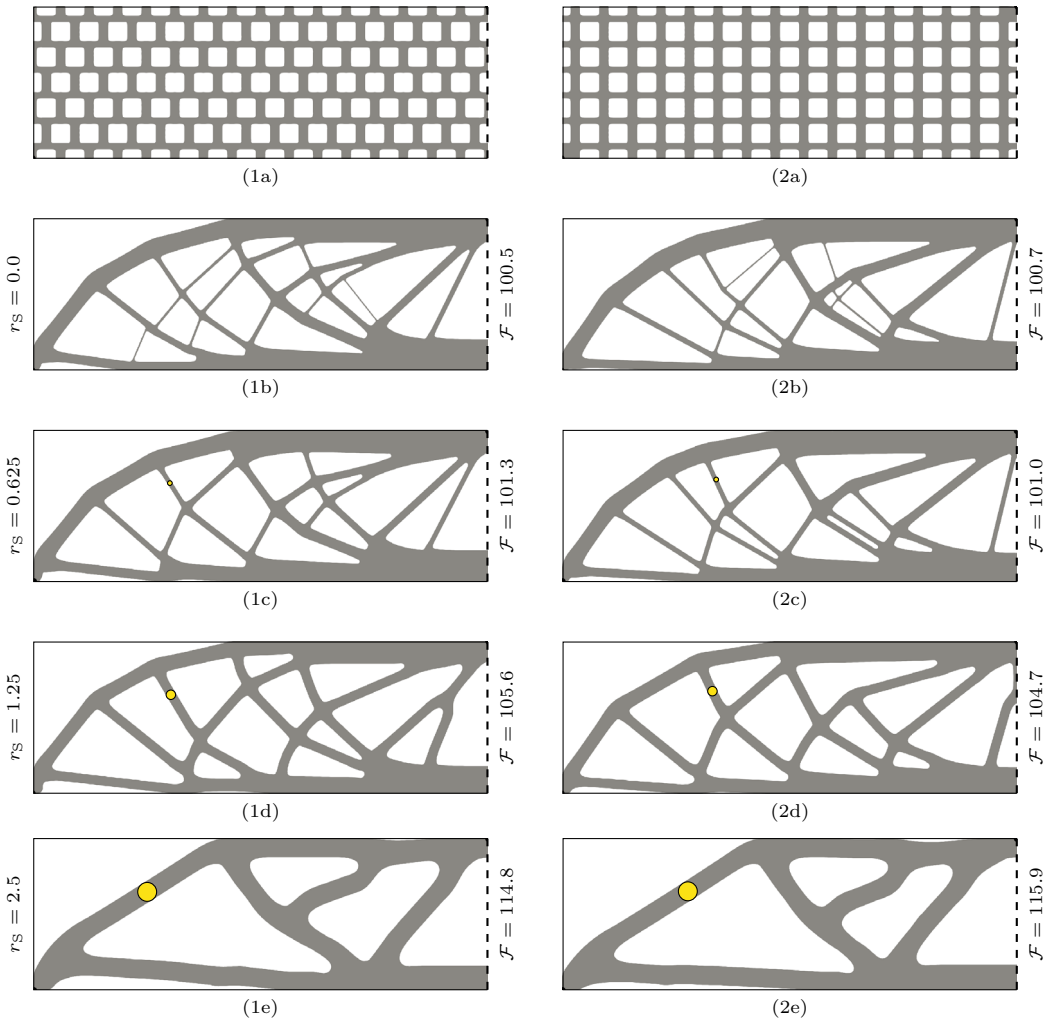

Fig. 11 2D beam design: Enforcing different length scales with spread radii $r_S = [0.0, 0.625, 1.25, 2.5]$ considering two initial configurations (1a) and (2a). Optimized designs are provided for problems without (**b**) and with (**c**)-(**e**) length scale control with strengthening and activation strategy

at half the design domain length. A cut in the $\mathbf{e}_x - \mathbf{e}_z$ plane, located at half the design domain height, is also provided. A yellow mark represents the imposed length scale and the compliance is given for each design.

The optimization results in designs that share a similar topology, but local differences are observable. Similarly to the 2D cases, both optimization problems yield designs that satisfy the imposed length scale. The activation strategy leads to a design consisting purely of shear webs, while truss-like connections are found without activation strategy, see the cross-section of a truss connection in the cut in the $\mathbf{e}_y - \mathbf{e}_z$ plane at a quarter of the design domain. These connections are structurally inferior to shear webs, as reported in Villanueva and Maute (2014), resulting in slightly inferior performance. Such truss-like connections remain in the final design, as the feature size penalty tends to inhibit topological changes. This effect is therefore still present in 3D, however, to a lesser extent than for the 2D case, where topological changes were fully inhibited in the absence of a continuation strategy. This observation validates the choice of a lower final continuation iteration I_F for 3D problems, as it speeds up the optimization process and reduces the required computational effort without drastic performance losses.

4.2.2 Enforcing different length scales

In this subsection, the capability of the proposed formulation in controlling the length scale for 3D problems is assessed and three different spread radii are considered $r_S = [1.25, 2.5, 5.0]$. Similarly to the 2D case, the penalty weight w_l is multiplied by the ratio $r_S/1.25$ to balance the difference in steepness of the spread skeleton. The continuation strategies on parameters μ_l and $\mathcal{S}_{th}$ are used and a final continuation iteration $I_F = 200$ is selected.

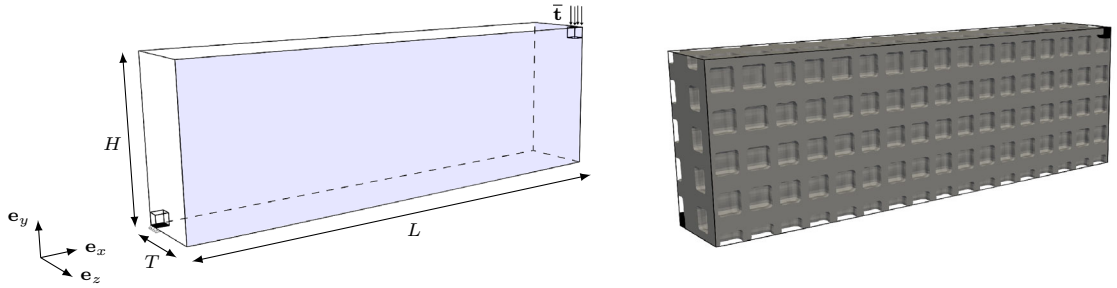

Fig. 12 3D beam design: geometry and boundary conditions (left), initial hole seeding (right)

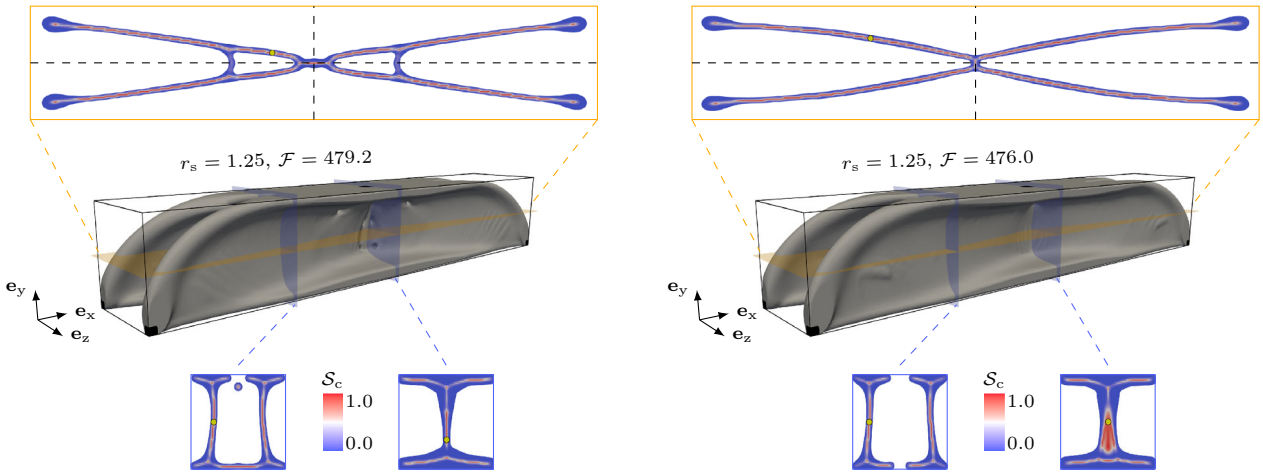

Fig. 13 3D beam design: Enforcing a length scale with $r_S = 1.25$ with (right) and without (left) strengthening and activation strategy

Figure 14 shows the optimized designs with and without length scale control. Along with the design layouts, two cuts in the $\mathbf{e}_y - \mathbf{e}_z$ plane and one cut in the $\mathbf{e}_x - \mathbf{e}_z$ are provided. A yellow mark represents the imposed length scale and performance in terms of compliance is given for each design.

While all optimized structures satisfy the required length scale, there are noticeable differences in their topologies. Trends analogous to the 2D case are observed in 3D. The smaller the filter radius, the closer is the resemblance to the design without feature size (top left), i.e., designs consisting primarily of shear webs. Enforcing a larger feature size results in a decrease in performance, as fine features cannot be developed, and shear webs cannot be sustained at the given feature size. As the length scale penalty is tightened and as wider regions of the design domain are being recruited, holes emerge within the shear webs and truss-like connections are developed. Designs made of a combination of shear webs and trusses are generated for $r_S = 2.5$ and made of only trusses for $r_S = 5.0$.

5 Conclusion

This paper presents a simple and efficient framework for imposing minimum length scale in level set-based TO using skeleton information. The design geometry is described via the level set method, while the structural analysis is based on the XFEM. The framework uses a novel approach to obtain a spread skeleton field that embeds the skeleton location and associated predefined thickness. The skeleton is derived from solving two computationally inexpensive auxiliary physics problems. The proposed method is applied to two- and three-dimensional structural solid/void TO problems considering compliance minimization under a volume constraint.

The numerical examples demonstrate the capability of the proposed methodology to accurately control the length scale for both two- and three-dimensional examples. Similarly to other level set-based feature size control schemes, the developed approach tends to impede topological changes and leads to a strong dependence on the initial design, especially in 2D. To promote significant design updates in the early stage of the optimization problems and avoid convergence to suboptimal solutions, continuation strategies, based on the spread skeleton information, are proposed to initially relax and later on tighten the enforcement of the length scale

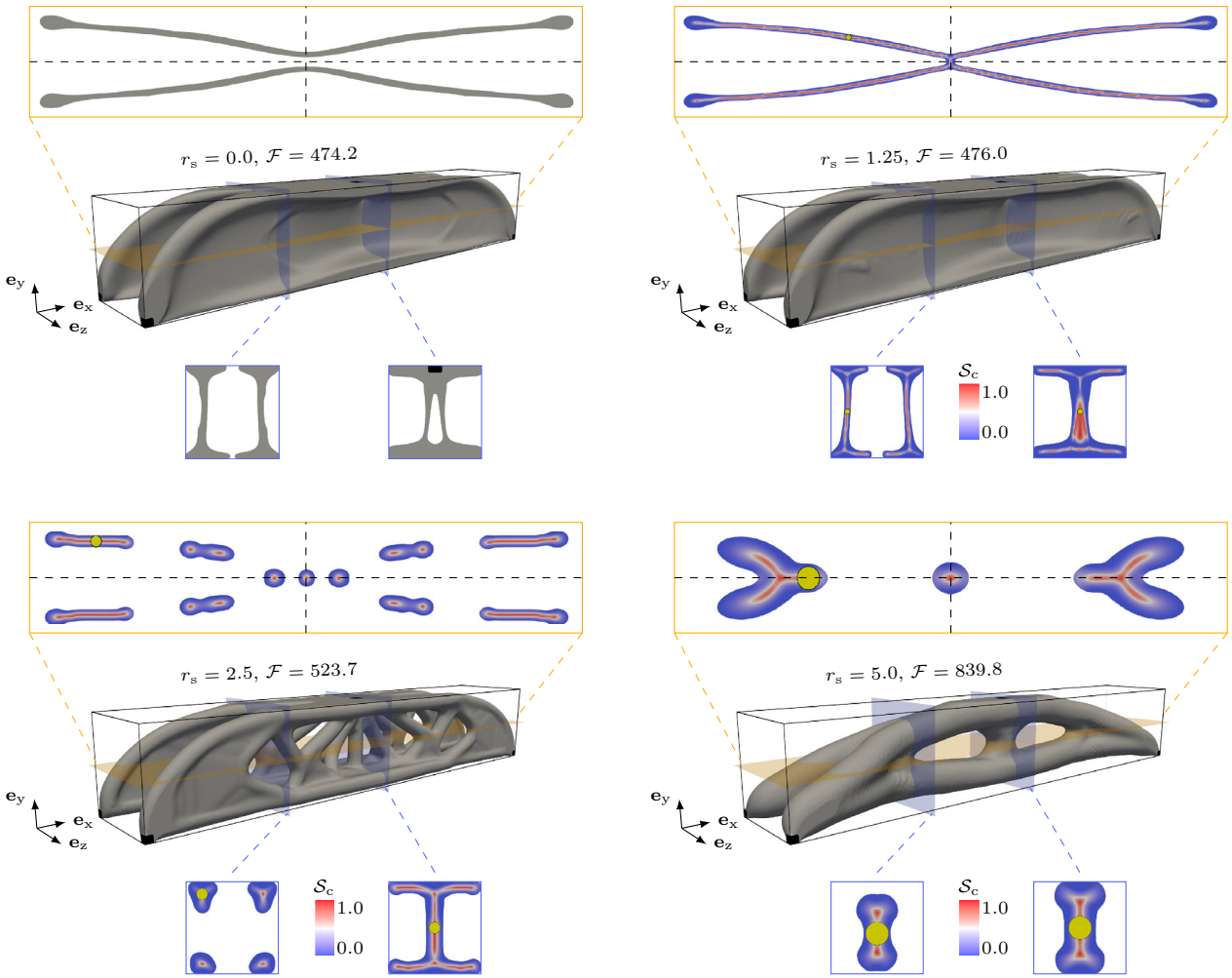

Fig. 14 3D beam design: Enforcing different length scales with spread radii $r_S = [0.0,\ 1.25,\ 2.5,\ 5.0]$ with strengthening and activation strategy

penalty. Numerical examples show that such continuations allow generating designs with enhanced performance at the required length scale. While the dependency on the initial configuration is mitigated, the latter is still observable and the resulting designs and convergence of the optimization problems are affected by the selection of the continuation parameters. Finally, numerical examples show that the proposed penalty not only enforces length scale, but also restricts the design geometry at junctions, thereby leading to the enforcement of a minimum corner radius.

The proposed spread skeleton shows potential to represent geometric properties of arbitrary shapes, making it an interesting approach to formulate various geometric constraints. Future work will focus on the following: (i) extending the framework to additional manufacturing constraints. For example, imposing uniform or maximum feature size could be achieved by penalizing design areas which lie too far away from the skeleton; (ii) decoupling the geometric restrictions imposed by the proposed thickness measure, i.e., minimum feature size and corner radius. Separating the effect of these constraints could be done by exploiting additional geometric or second-order gradient information; and (iii) extending the proposed approach to more complex physics, where length scale control can be crucial for the accuracy of the predicted physics responses.

Author Contributions The conceptual design and implementation of the presented research were performed by both authors. Numerical studies were carried out by N. Hermann. Both authors contributed to writing the first draft of the manuscript and to its revision. L. Noël supervised the presented work. Both authors read and approved the final manuscript.

Funding No funds, grants, or other support was received.

Data Availability The numerical studies presented in this paper used the open-source software MORIS (2025), available at https://github.com/kkmaute/moris.

Code Availability The authors will provide the set of input parameters and meshes for each topology optimization problem presented in the paper upon request.

Declarations

Conflict of interest On behalf of all authors, the corresponding author states that there is no conflict of interest.

References

Aage N, Giele R, Andreasen C (2021) Length scale control for high-resolution three-dimensional level set–based topology optimization. Struct Multidiscip Optim 64(3):1127–1139. https://doi.org/10.1007/s00158-021-02904-4

Allaire G, Jouve F, Toader A-M (2004) Structural optimization using sensitivity analysis and a level-set method. J Comput Phys 194(1):363–393. https://doi.org/10.1016/j.jcp.2003.09.032

Allaire G, Jouve F, Michailidis G (2016) Thickness control in structural optimization via a level set method. Struct Multidiscip Optim 53(6):1349–1382. https://doi.org/10.1007/s00158-016-1453-y

Amestoy P, Duff IS, Koster J, L'Excellent J-Y (2001) A fully asynchronous multifrontal solver using distributed dynamic scheduling. SIAM J Matrix Anal Appl 23(1):15–41. https://doi.org/10.1137/S0895479899358194

Andreasen C, Elingaard M, Aage N (2020) Level set topology and shape optimization by density methods using cut elements with length scale control. Struct Multidiscip Optim 62:685–707. https://doi.org/10.1007/s00158-020-02527-1

Barrera JL, Geiss MJ, Maute K (2020) Hole seeding in level set topology optimization via density fields. Struct Multidiscip Optim 61:1319–1343. https://doi.org/10.1007/s00158-019-02480-8

Barrera JL, Geiss MJ, Maute K (2022) Minimum feature size control in level set topology optimization via density fields. Struct Multidiscip Optim 65(3):94. https://doi.org/10.1007/s00158-021-03096-7

Bavier E, Hoemmen M, Rajamanickam S, Thornquist H (2012) Amesos2 and belos: direct and iterative solvers for large sparse linear systems. Sci Program 20(3):243875. https://doi.org/10.3233/SPR-2012-0352

Belyaev AG, Fayolle P-A (2015) On variational and pde-based distance function approximations. Computer Graphics Forum 34(8):104–118. https://doi.org/10.1111/cgf.12611

Belytschko T, Black T (1999) Elastic crack growth in finite elements with minimal remeshing. Int J Numer Meth Eng 45(5):601–620. https://doi.org/10.1002/(sici)1097-0207(19990620)45:5<601::aid-nme598>3.0.co;2-s

Bendsøe MP, Kikuchi N (1988) Generating optimal topologies in structural design using a homogenization method. Comput Methods Appl Mech Eng 71:197–224. https://doi.org/10.1016/0045-7825(88)90086-2

Blum H (1967) A Transformation for Extracting New Descriptors of Shape. In: Wathen-Dunn W (ed) Models for the Perception of Speech and Visual Form. MIT Press, Cambridge

Blum H (1973) Biological shape and visual science (part i). J Theor Biol 38(2):205–287. https://doi.org/10.1016/0022-5193(73)90175-6

Bourdin B (2001) Filters in topology optimization. Int J Numer Meth Eng 50(9):2143–2158. https://doi.org/10.1002/nme.116

Bruns TE, Tortorelli DA (2001) Topology optimization of non-linear elastic structures and compliant mechanisms. Comput Methods Appl Mech Eng 190(26):3443–3459. https://doi.org/10.1016/S0045-7825(00)00278-4

Burman E (2010) Ghost penalty. CR Math 348(21):1217–1220. https://doi.org/10.1016/j.crma.2010.10.006

Carstensen JV, Guest JK (2018) Projection-based two-phase minimum and maximum length scale control in topology optimization. Struct Multidiscip Optim 58:1845–1860. https://doi.org/10.1007/s00158-018-2066-4

Chen S, Wang M, Liu A (2008) Shape feature control in structural topology optimization. Comput Aided Des 40(9):951–962. https://doi.org/10.1016/j.cad.2008.07.004

Clausen A, Aage N, Sigmund O (2015) Topology optimization of coated structures and material interface problems. Comput Methods Appl Mech Eng 290:524–541. https://doi.org/10.1016/j.cma.2015.02.011

Crane K, Weischedel C, Wardetzky M (2017) The heat method for distance computation. Commun ACM 60(11):90–99. https://doi.org/10.1145/3131280

Deaton JD, Grandhi RV (2014) A survey of structural and multidisciplinary continuum topology optimization: post 2000. Struct Multidiscip Optim 49(1):1–38. https://doi.org/10.1007/s00158-013-0956-z

Dunning P (2018) Minimum length-scale constraints for parameterized implicit function based topology optimization. Struct Multidiscip Optim 58:155–169. https://doi.org/10.1007/s00158-017-1883-1

Fernández E, Yang K, Koppen S, Alarcón P, Bauduin S, Duysinx P (2020) Imposing minimum and maximum member size, minimum cavity size, and minimum separation distance between solid members in topology optimization. Comput Methods Appl Mech Eng 368:113157. https://doi.org/10.1016/j.cma.2020.113157

Geiss M (2018) *Level-set-XFEM-density topology optimization of active structures: Methods and applications*. PhD thesis, University of Colorado Boulder

Geiss MJ, Maute K (2018) Topology optimization of active structures using a higher-order level-set-XFEM-density approach. Multidisc Anal Opt Conf. https://doi.org/10.2514/6.2018-4053

Geiss MJ, Barrera JL, Boddeti N, Maute K (2019) A regularization scheme for explicit level-set XFEM topology optimization. Front Mech Eng 14(2):153–170. https://doi.org/10.1007/s11465-019-0533-2

Guest JK (2009) Imposing maximum length scale in topology optimization. Struct Multidiscip Optim 37:463–473. https://doi.org/10.1007/S00158-008-0250-7/METRICS

Guest JK (2009) Topology optimization with multiple phase projection. Comput Methods Appl Mech Eng 199:123–135. https://doi.org/10.1016/j.cma.2009.09.023

Guest JK, Prévost JH, Belytschko T (2004) Achieving minimum length scale in topology optimization using nodal design variables and projection functions. Int J Numer Meth Eng 61(2):238–254. https://doi.org/10.1002/nme.1064

Guo X, Zhang W, Zhong W (2014) Explicit feature control in structural topology optimization via level set method. Comput Methods Appl Mech Eng 272:354–378. https://doi.org/10.1016/j.cma.2014.01.010

Haber RB, Jog CS, Bendsøe MP (1996) A new approach to variable-topology shape design using a constraint on perimeter. Structural optimization 11(1):1–12. https://doi.org/10.1007/bf01279647

Huang J, Liu J (2024) Derivable skeletons in topology optimization for length scale control. Comput Methods Appl Mech Eng 421:116778. https://doi.org/10.1016/j.cma.2024.116778

Jansen M (2019) Explicit level set and density methods for topology optimization with equivalent minimum length scale constraints. Struct Multidiscip Optim 59:1775–1788. https://doi.org/10.1007/s00158-018-2162-5

Lazarov B, Sigmund O (2011) Filters in topology optimization based on helmholtz-type differential equations. Int J Numer Meth Eng 86(6):765–781. https://doi.org/10.1002/nme.3072

Lazarov B, Wang F, Sigmund O (2016) Length scale and manufacturability in density-based topology optimization. Arch Appl Mech 86(1):189–218. https://doi.org/10.1007/s00419-015-1106-4

Liu J, Ma Y (2016) A survey of manufacturing oriented topology optimization methods. Adv Eng Softw 100:161–175. https://doi.org/10.1016/j.advengsoft.2016.07.017

Liu J, Ma Y, Fu J, Duke K (2015) A novel cacd/cad/cae integrated design framework for fiber-reinforced plastic parts. Adv Eng Softw 87:13–29. https://doi.org/10.1016/j.advengsoft.2015.04.013

Liu J, Yu H, Ma Y (2016) Minimum void length scale control in level set topology optimization subject to machining radii. Comput Aided Des 81:70–80. https://doi.org/10.1016/J.CAD.2016.09.007

Liu J, Li L, Ma Y (2018) Uniform thickness control without prespecifying the length scale target under the level set topology optimization framework. Adv Eng Softw 115:204–216. https://doi.org/10.1016/j.advengsoft.2017.09.013

Luo J, Luo Z, Chen S, Tong L, Wang MY (2008) A new level set method for systematic design of hinge-free compliant mechanisms. Comput Methods Appl Mech Eng 198:318–331. https://doi.org/10.1016/j.cma.2008.08.003

Makhija D, Maute K (2014) Numerical instabilities in level set topology optimization with the extended finite element method. Struct Multidiscip Optim 49:185–197. https://doi.org/10.1007/s00158-013-0982-x

Menten M J, Paetzold J C, Zimmer V A, Shit S, Ezhov I, Holland R, Probst M, Schnabel J A, Rueckert D (2023) A skeletonization algorithm for gradient-based optimization. In *Proceedings of the IEEE/CVF International Conference on Computer Vision (ICCV)*, pages 21394–21403, October

Michailidis G (2014) *Manufacturing Constraints and Multi-Phase Shape and Topology Optimization via a Level-Set Method*. PhD thesis, Ecole Polytechnique X. URL http://pastel.archives-ouvertes.fr/pastel-00937306

Mommeyer C, Lombaert G, Schevenels M, Sigmund O (2024) Taylor series approximations for fasterrobust topology optimization. Struct Multidiscip Optim 67:181. https://doi.org/10.1007/s00158-024-03890-z

Montero A S, Lang J (2012) Skeleton pruning by contour approximation and the integer medial axistransform. In: Computers and Graphics (Pergamon). 36:477-487. https://doi.org/10.1016/j.cag.2012.03.029

MORIS (2025) Multi-physics optimization research and innovation system. URL https://github.com/kkmaute/moris. Accessed on 2025-08-21

Nitsche J (1971) Über ein Variationsprinzip zur Lösung von Dirichlet-Problemen bei Verwendung von Teilräumen, die keinen Randbedingungen unterworfen sind. Abh Math Semin Univ Hambg 36:9–15

Noël L, Schmidt M, Messe C, Evans J, Maute K (2020) Adaptive level set topology optimization using hierarchical B-splines. Struct Multidiscip Optim 62(4):1669–1699. https://doi.org/10.1007/s00158-020-02584-6

Noël L, Schmidt M, Doble K, Evans J, Maute K (2022) Xiga: an extended isogeometric analysis approach for multi-material problems. Comput Mech 70(6):1281–1308. https://doi.org/10.1002/nme.3072

Osher S, Sethian JA (1988) Fronts propagating with curvature-dependent speed: algorithms based on hamilton-jacobi formulations. J Comput Phys 79(1):12–49. https://doi.org/10.1016/0021-9991(88)90002-2

Petersson J, Sigmund O (1998) Slope constrained topology optimization. Int J Numer Meth Eng 41(8):1417–1434. https://doi.org/10.1002/(SICI)1097-0207(19980430)41:8<1417::AID-NME344>3.0.CO;2-N

Poulsen T (2003) A new scheme for imposing a minimum length scale in topology optimization. Int J Numer Meth Eng 57(6):741–760. https://doi.org/10.1002/nme.694

Saha PK, Borgefors G, di Baja GS (2016) A survey on skeletonization algorithms and their applications. Pattern Recogn Lett 76:3–12. https://doi.org/10.1016/J.PATREC.2015.04.006

Schevenels M, Lazarov B, Sigmund O (2011) Robust topology optimization accounting for spatially varying manufacturing errors. Comput Methods Appl Mech Eng 200(49):3613–3627. https://doi.org/10.1016/j.cma.2011.08.006

Sethian J, Wiegmann A (2000) Structural boundary design via level set and immersed interface methods. J Comput Phys 163(2):489–528. https://doi.org/10.1006/jcph.2000.6581

Sharma A, Villanueva H, Maute K (2017) On shape sensitivities with heaviside-enriched XFEM. Struct Multidiscip Optim 55(2):385–408. https://doi.org/10.1007/s00158-016-1640-x

Siddiqi K, Pizer S (2008) Medial representations: mathematics, algorithms and applications. Computational Imaging and Vision, Springer, Dordrecht. Edition 1. ISBN 978-1-4020-8657-1

Sigmund O (1997) On the design of compliant mechanisms using topology optimization. J Struct Mech 25:493–524. https://doi.org/10.1080/08905459708945415

Sigmund O (2009) Manufacturing tolerant topology optimization. Acta Mech Sin 25(2):227–239. https://doi.org/10.1007/s10409-009-0240-z

Sigmund O, Maute K (2013) Topology optimization approaches-A comparative review. Struct Multidiscip Optim 48(6):1031–1055. https://doi.org/10.1007/s00158-013-0978-6

Stankiewicz G, Dev C, Steinmann P (2021) Coupled topology and shape optimization using an embedding domain discretization method. Struct Multidiscip Optim 64:2687–2707. https://doi.org/10.1007/s00158-021-03024-9

Svanberg K (2002) A class of globally convergent optimization methods based on conservative convex separable approximations. SIAM J Optim 12(2):555–572. https://doi.org/10.1016/0021-9045(72)90080-9

van Dijk NP, Maute K, Langelaar M, van Keulen F (2013) Level-set methods for structural topology optimization: a review. Struct Multidiscip Optim 48(3):437–472. https://doi.org/10.1007/s00158-013-0912-y

Vatanabe SL, Lippi TN, Lima CR, Paulino GH, Silva EC (2016) Topology optimization with manufacturing constraints: a unified projection-based approach. Adv Eng Softw 100:97–112. https://doi.org/10.1016/J.ADVENGSOFT.2016.07.002

Villanueva CH, Maute K (2014) Density and level set-XFEM schemes for topology optimization of 3-d structures. Comput Mech 54(1):133–150. https://doi.org/10.1007/s00466-014-1027-z

Wang F, Lazarov BS, Sigmund O (2011) On projection methods, convergence and robust formulations in topology optimization. Struct Multidiscip Optim 43:767–784. https://doi.org/10.1007/S00158-010-0602-Y/FIGURES/21

Wang MY, Wang X, Guo D (2003) A level set method for structural topology optimization. Comput Methods Appl Mech Eng

192(1):227–246. https://doi.org/10.1016/s0045-7825(02)00559-5

Wang Y, Zhang L, Wang M (2016) Length scale control for structural optimization by level sets. Comput Methods Appl Mech Eng 305:891–909. https://doi.org/10.1016/j.cma.2016.03.037

Wang Y, Hu T, Zou Z, Wang Y, Zhang X (2025) Constraint-free length scale control for topology optimization using the velocity field level set method. Struct Multidiscip Optim. https://doi.org/10.1007/s00158-025-03971-7

Wei P, Wang W, Yang Y, Wang MY (2020) Level set band method: a combination of density-based and level set methods for the topology optimization of continuums. Front Mech Eng 15:390–405. https://doi.org/10.1007/s11465-020-0588-0

Wunsch N, Doble K, Schmidt MR, Noël L, Evans JA, Maute K (2025) Enriched immersed finite element and isogeometric analysis: algorithms and data structures. Eng Comput. https://doi.org/10.1007/s00366-025-02163-7

Xia Q, Shi T (2015) Constraints of distance from boundary to skeleton: for the control of length scale in level set based structural topology optimization. Comput Methods Appl Mech Eng 295:525–542. https://doi.org/10.1016/j.cma.2015.07.015

Yamada T (2019a) Thickness constraints for topology optimization using the fictitious physical model. In *EngOpt 2018 Proceedings of the 6th International Conference on Engineering Optimization*. Springer International Publishing

Yamada T (2019) Geometric shape features extraction using a steady state partial differential equation system. J Comput Design Eng 6(4):647–656. https://doi.org/10.1016/j.jcde.2019.03.006

Zhang W, Zhong W, Guo X (2014) An explicit length scale control approach in simp-based topology optimization. Comput Methods Appl Mech Eng 282:71–86. https://doi.org/10.1016/J.CMA.2014.08.027

Zhou M, Lazarov B, Wang F, Sigmund O (2015) Minimum length scale in topology optimization by geometric constraints. Comput Methods Appl Mech Eng 293:266–282. https://doi.org/10.1016/j.cma.2015.05.003

Zobaer T, Sutradhar A (2023) Maximum thickness control in topology optimization using an inflection-point-based geometric constraint. Comput Methods Appl Mech Eng 414:116171. https://doi.org/10.1016/J.CMA.2023.116171